Nanometer-Scale Metallic Grains Connected with Atomic-Scale Conductors

A. Anaya, A. L. Korotkov, M. Bowman, J. Waddell, and D. Davidovic,*
Georgia Institute of Technology, Atlanta, GA 30332
(Dated: February 1, 2008)

We describe a technique for connecting a nanometer-scale gold grain to leads by atomic-scale gold point contacts. These devices differ from previous metallic quantum dots in that the conducting channels are relatively well-transmitting. We investigate the dependence of the Coulomb blockade on contact resistance. The high-resistance devices display Coulomb blockade and the low-resistance devices display a zero-bias conductance dip, both in quantitative agreement with theory. We find that in the intermediate regime, where the sample resistance is close to h/e^2, the I-V curve displays a Coulomb staircase with symmetric contact capacitances.

INTRODUCTION

Fabrication of nanometer scale devices has recently become a subject of intensive study. In nanometer-scale metallic devices, discrete electronic energy levels can be resolved at low temperatures. The effects of discrete electronic levels on quantum transport in small metallic samples have been observed in atomic contacts and in nanometer scale grains.

Atomic contacts have been created using scanning probe microscopes [1] and mechanically controlled break junctions [2, 3]. In these techniques, a metallic contact is broken, for example by elongation, and one measures the conductance versus elongation. The combination of two effects, conductance quantization [4, 5] and sudden rearrangements of the atomic structure [6, 7], cause the conductance to decrease in discrete steps while the contacts are stretched to the breaking point. The steps are on the order of the conductance quantum $G_0 = 2e^2/h$.

In metallic grains, a single grain has been placed in weak tunneling contact with source and drain leads, [8, 9] creating a single electron transistor (SET). [10] At dilution refrigerator temperature, discrete energy levels of the grain are measured from the I-V curve. The discrete energy spectra are analogous to those in artificial atoms. [11, 12, 13]

Study of both atomic scale contacts and grains has led to major advances in understanding quantum transport in metals. For an extensive review of quantum properties of atomic-scale conductors and grains see Refs. [14] and [15], respectively.

In this paper, we describe a technique to connect one gold grain to drain and source by atomic scale contacts. The samples that we generate demonstrate behaviors of both atomic contacts and metallic grains. We show that the contact conductances can be changed in discrete steps of size comparable with G_0, showing that the conductance channels are well transmitting. This property differentiates our new devices from previously studied grains. [15] We investigate the Coulomb blockade of a grain as a function of the contact conductance. We identify a regime of intermediate Coulomb blockade, where the sample resistance is close to the resistance quantum.

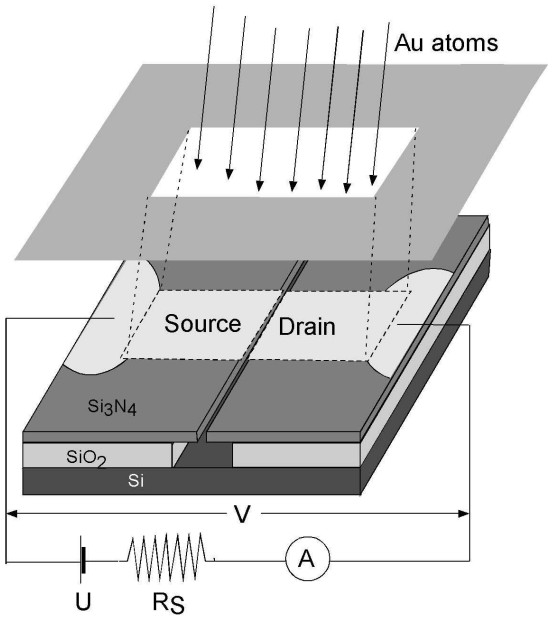

FIG. 1: Metal deposition process for creating a point contact and/or a grain connected between the source and the drain. The gap between Si_3N_4 substrates is 70nm, the width of the undercut in SiO_2 is 120nm.

EXPERIMENTAL SETUP

The samples are created by combining metal deposition and electric field induced surface migration of gold. Recently, an electromigration technique has been implemented in fabrication of metallic electrodes with nanometer separation by Park et al. [16] In this technique a gold nanowire had been made by electon-beam lithography, then broken by passing large current through it. The current flow had caused the electromigration of gold atoms, and the nanowire to break. An electromigration technique was subsequently applied at cryogenic temper-

atures, [17] which lead to the fabrication of atomic scale transistors.

Our technique is different from that of Park et al., in that a strong electric field is applied to create a connection between two separate gold leads; it is based on electric field induced surface migration, [18] which is different from electromigration.

A $5N$ purity gold film is deposited on to two insulating Si_3N_4 substrates separated by a 70 nm slit, as shown in Fig. 1, in vacuum of $\sim 10^{-6}$ torr. The slit has a large undercut in SiO_2, which prevents electrical contact between the films. The exposed length of the slit is 0.1 mm.

Electric current across the slit is monitored during the deposition. The applied voltage is U and the voltage source impedance is R_S. When the thickness of the film is near $\sim 80nm$, an electric contact between drain and source appears abruptly.

The contact between the drain and the source forms at a random location along the exposed length of the slit. The nature of the contact depends on R_S, U, the amount of gold deposited after the contact is detected, vapor pressure and temperature. The devices that can be obtained by this technique are metallic point contacts, tunneling junctions, and grains.

METALLIC POINT CONTACTS

To create a metallic point contact, we set $R_S = 0$ and $U \leq 0.1$ V. Once the slightest conductance is detected, deposition is stopped. With further gold deposition the conductance would increase rapidly and display discrete steps in conductance versus time, of size $\sim G_0$.

In some samples, stable contacts with conductance comparable with G_0 can be obtained by stopping the metal deposition at the right time. These contacts are stable for minutes or longer.

Frequently, it is impossible to stop the deposition when the contact conductance is near G_0, because the contact conductance jumps to a value of $\sim 100G_0$. In addition, the contacts that have conductance of order G_0 often suddenly jump into this $100G_0$ state or they disconnect.

PLANAR TUNNELING BARRIERS

Intuition suggests that if two gold surfaces are in mechanical contact, then there should also exist a good electrical contact. In this section, we show that mechanical contact does not necessarily imply a good electrical contact. It is possible to create a stable planar tunneling junction between two gold surfaces, with large tunneling resistance. This tunneling barrier is created if the gold surface contains adsorbates.

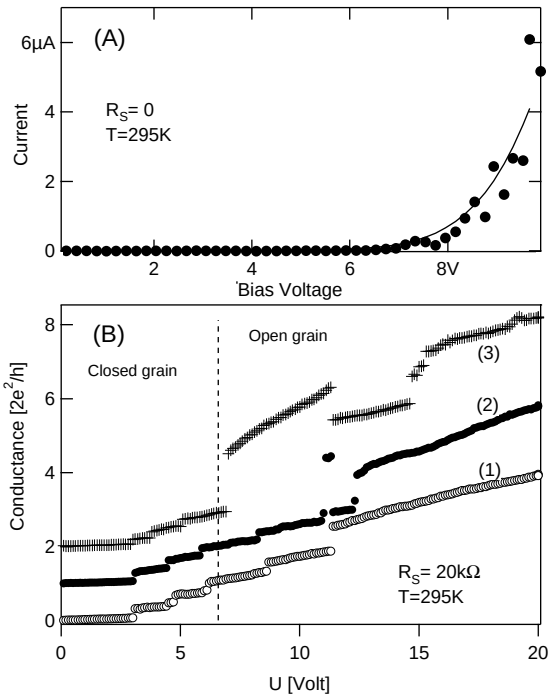

FIG. 2: A. Circles: $I-V$ curve of a contact taken immediately after detecting the slightest current at 10 V bias. Line: Fit to an $I-V$ curve of a tunneling junctions. The fit parameters are $S = 2 \times 10^3 nm^2$,$d = 7.5\mathring{A}$, and $\Delta = 6.4$ eV for the junction area S, gap size d, and the barrier height Δ. B. Increasing the contact conductance by increasing U in Fig. 1 with $R_S = 20k\Omega$. Three curves are obtained in three samples. The curves are offset by $2e^2/h$ in vertical direction for clarity. These conductance traces are analogous to those found in break-junctions. [14]

Planar tunneling barriers between gold surfaces have been first proposed by Hansen et al. [19, 20] The authors observe that gold metallic contacts of conductance $\sim G_0$ grown in ultrahigh vacuum are much less stable than intentionally contaminated contacts with the same conductance. The enhanced stability is explained by a tunneling barrier composed of adsorbates, which has a mechanical contact area much larger than that for a metallic contact with the same conductance. The dimensions of these barriers are obtained by fitting the I-V curves. They vary from $\sim 12nm$ to $\sim 50nm$. The thickness of the barrier is of order several $\mathring{A}$.

We confirm this proposal in our experimental setup and clarify the conditions under which different types of contacts form. Since the pressure during the metal deposition is 10^{-6} Torr, the surfaces contain adsorbates. The nature of the contact that forms at this pressure depends on the applied voltage.

If the applied voltage is weak ($U < 0.1$ V), then the contacts are metallic, as described in the previous section. If the voltage is large, ($U > 5$ V and $R_S = 0$), the device contains a planar tunneling barrier and there is no direct

metallic connection between drain and source.

If the applied voltage is between 1 V and 3 V, the contacts are mixed between the above two cases. They contain a large tunneling barrier and a small metallic contact somewhere inside the barrier. These contacts have the advantage of having high stability and high channel transmittance. They are described in a separate section.

We discuss the high voltage regime first. We return to the deposition process in Fig. 1 with $U = 10$ V and $R_S = 0$. When the Au film thickness reaches ~ 80 nm, the current suddenly jumps to a nonzero value.

The conductance (I/V) strongly fluctuates in time. The average I/V is much smaller than G_0. As soon as the contact is detected, we stop metal deposition and reduce the bias voltage close to zero. We minimize the time that the devices are exposed to 10 V to about one second.

While reducing the voltage, at a rate of one volt in ten millisecond, we measure the I-V curve. A typical I-V curve is shown in Fig. 2-A. It is relatively well modeled by the I-V curve of a single tunneling junction [21] with the barrier height comparable to the gold work function $W_{Au} = 5.1$ eV. The diameter of the barrier is ~ 10 nm, consistent with ref. [19, 20].

The barrier height is slightly larger than W_{Au}. This is explained by significant contamination of the junctions with adsorbates, such as H_2O. [32]

We image the contacts by the scanning electron microscope (SEM). Transferring the sample from the deposition chamber to another instrument almost certainly leads to a sudden increase in resistance to an undetectably high value, despite being grounded at both ends during transfer. In most samples, the electrical contact can be reestablished by applying a one second long voltage pulse at 10 V (or sometimes higher) in high vacuum. The sample returns to the high resistance tunneling barrier.

Figure 3-A shows one gold grain in mechanical contact with the source. The sample disconnected spontaneously while transferring to the SEM as described above. We apply the voltage pulse, while imaging and measuring the current simultaneously. The current starts to flow during the pulse duration. After the pulse, the sample resistance at low bias is $\sim 1G\Omega$ or higher.

Figure 3 B shows the device after the voltage pulse. We verify through microscopy that no additional connections are formed outside the slit in Figure 3. The mechanical contact area is of order 10 nm, confirming the proposal by Hansen et al.

Under the influence of voltage, the grain pulled a Au protrusion from the right lead, establishing contact. This protrusion forms because of a process known as electric field induced surface migration, see Ref. [18] and references therein.

It is understood that the protrusion grows because of a force acting on surface gold atoms. When the electric field exceeds a certain threshold, it leads to migration of surface gold atoms toward the region of the strongest electric field, creating a protrusion. The protrusion increases the electric field gradient, which in turn accelerates its growth. When the protrusion reaches the other side, a planar junction is formed. This junction is stable after the voltage is reduced.

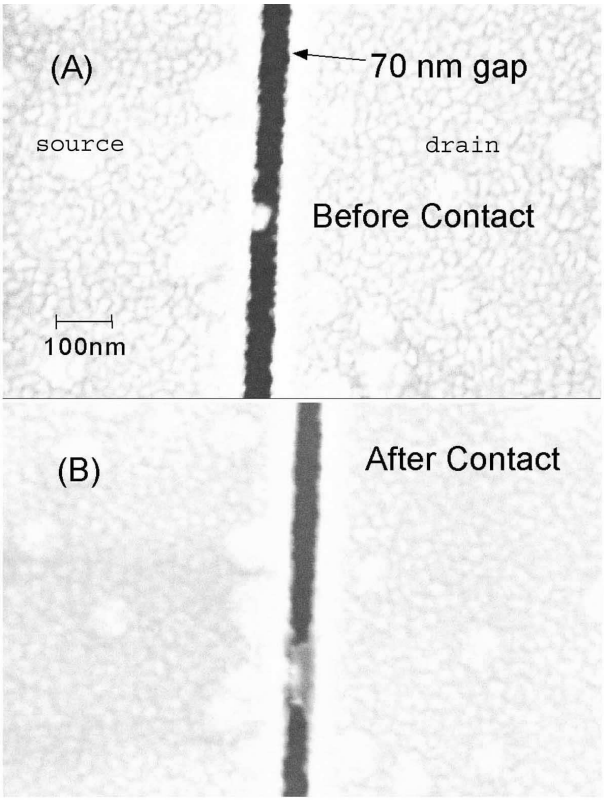

FIG. 3: A. One gold grain attached to one lead. B. The grain after applying the 10 volt pulse.

FORMATION OF GRAINS IN ELECTRIC BREAKDOWN

Consider a metallic point contact with resistance less than 10Ω. We apply a voltage pulse of 10 V in vacuum. The contact breaks down, and after the pulse the resistance is immeasurably large.

We observe the break-down by the SEM. Fig. 4-A shows an area near the contact after the break down. Evidently, a relatively wide region around the point contact melts under the influence of the voltage pulse. The molten gold retracts away from the slit, presumably in order to reduce surface energy.

In addition, a large number of electrically isolated grains is left behind on the substrate surface. This is shown in fig. 4-B. The image indicates a broad distribution of grain diameters. The particles have nearly cir-

cular shape. This suggests that the particles have been molten (in the liquid state, minimizing the surface energy in contact with the substrate leads to circular grains).

PLANAR TUNNELING BARRIERS - REVISITED

In Fig. 3-B, there is a grain between drain and source. The majority of devices fabricated with a 10 V pulse, as in fig. 3-B, have I-V curves that exhibit the Coulomb staircase at low temperatures. Since the staircase is conditional on $R_L, R_R > h/e^2$, where R_L and R_R are the contact resistances between the grain and the leads, this shows that there are at least two contacts in series between drain and source. In later sections, when we discuss Coulomb Blockade, we infer from the I-V curves that there is only one grain between the drain and the source. Figure 3-B supports this conclusion.

We propose the following scenario for grain formation. We suggest that the very first contact at 10 V bias voltage is metallic. It lasts only for a very short time, because it breaks down by melting. During the break down, one or several grains are created analogous to Fig. 4.

MIXED CONTACTS

After creating a device with a 10 V pulse, as in fig. 3-B, we change the circuit in Fig. 1, so that $R_S = 20k\Omega$ and slowly increase U from zero, and measure the conductance (I/V). Note that U is the total voltage across the sample in series with R_S. Figure 2-B shows the resulting conductance traces in 3 different samples.

I/V jumps to a significant fraction of $2e^2/h$ at roughly 2.8 V. After the jump, the voltage across the sample V is reduced below U by voltage division with R_S, and the sample voltage becomes close to 1.7 V. Further increase in U results in two effects: there are additional discontinuities in conductance, of amplitude 0.2 to $2e^2/h$, and there is a smooth increase in conductance versus U. The increase in conductance is maintained if the voltage U is removed.

The discontinuities in conductance of size $\sim e^2/h$ suggest that discrete atomic reconfigurations take place, analogous to those in atomic conductors. [14] The steps demonstrate that the contacts contain well transmitting channels. In Fig. 3-B, the atomic scale contacts form somewhere inside the tunneling barrier between the grain and the leads.

The smooth conductance increase suggests that the tunneling contribution is increasing. We confirm through microscopy that the area of the planar barrier is increasing while the contact conductance is increasing smoothly.

As described before, in a strong nonuniform electric field, at room temperature, surface gold atoms move toward the strongest electric field. [18] We propose that

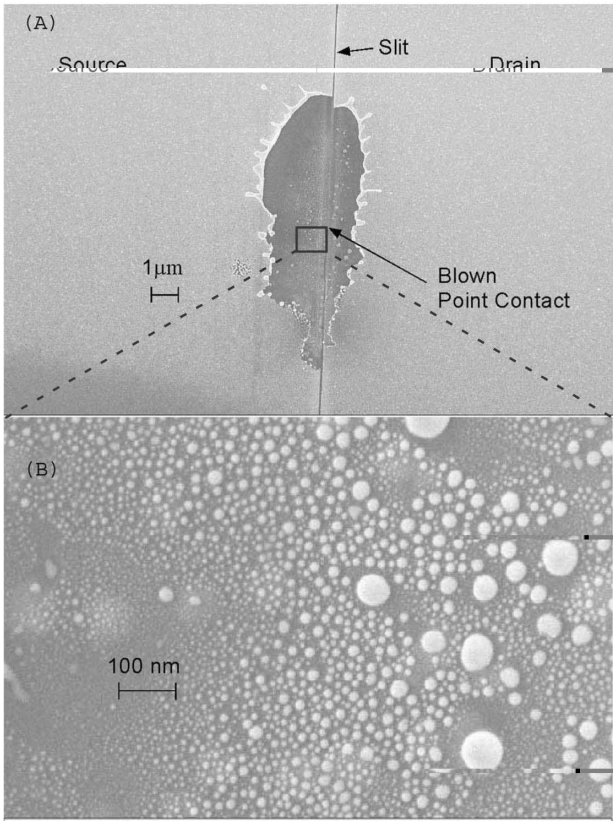

FIG. 4: A. Scanning Electron Microscope image of a metallic point contact after the electric breakdown by the voltage pulse, as described in the text B. A zoomed-in image of the blown region on the left side of the slit. An array of circular gold grains is left on the substrate.

when the electric field strength increases beyond a certain point, one atom pushes through the barrier, creating a metallic contact.

Once the first atom is connected, further increase in the electric field adds more gold atoms into the contact, increasing the number of channels and the conductance in steps of size $\sim e^2/h$.

These discrete atomic additions occur in both barriers. In fact, since the voltage drop is stronger at the higher resistance junction, and voltage drop drives the conductance increase, it follows that the increase in conductance tends to even out any imbalance between the two resistances. This balancing of the electric field leads to the desired property that the Coulomb blockade at low temperature vanishes in a relatively narrow range of sample resistance.

COULOMB BLOCKADE

To observe Coulomb Blockade, a sample whose resistance at room temperature is greater than or equal to 20 kΩ must be cooled to milliKelvin temperatures. How-

ever, the evaporator in which each sample is prepared cannot be cooled. So each sample must be moved to a dilution refrigerator where it can be cooled to as low as 10mK.

The samples are very sensitive to electrostatic shock and so a careful grounding procedure must be followed to safely transfer each sample from the chamber to the refrigerator. From outside the chamber, before venting to atmosphere, the voltage on the sample is reduced to zero, and both leads are grounded. After venting, a mobile grounding strap grounds the removable deposition stage, and the sample leads are grounded to the stage, where now the voltage leads to the outside circuitry may be safely removed. The stage may now move to an ESD-safe workstation (table) and the sample dismounted.

To dismount the sample from the stage, a small piece of indium wire is used to shunt the contact pads on the chip. Leads running from the stage to chip may now be disconnected. The chip is free to move to a stage more suitable for the dilution refrigerator. A small chip carrier, designed for use in the tailpiece of the refrigerator will house the sample. Leads from the carrier to the chip are connected by indium pressing to the contact pads. The leads, from the top of the refrigerator to a connector at the tailpiece, are grounded, and the carrier is finally attached to the connector. The indium shunt on the chip is removed. The sample is now available for cool down. Only through this laborious grounding procedure can we move samples and have them survive.

We have recently added the gate to our samples. To this end, the mask is placed back over the chip, but rotated by 90 degrees. Then the sample is returned to the deposition chamber and reconnected to the outside electronics. If the resistance of the sample is infinite, the sample is reconnected in high vacum, as in Fig. 3. Then, we deposit a layer of Al_2O_3, by reactive evaporation of aluminum. [9] Aluminum is deposited at angles of ± 5 deg relative to the substrate normal. For each angle, the deposited thickness is 15nm. Then, we deposit a layer of aluminum metal, 40 nm thick, in the direction parallel with the normal.

The refridgerator is closed and pumped down to $\sim 10^{-5}$ Torr. Then, the sample resistance is modified (if needed), using the techniques described in previous sections. Finally, the sample is cooled to 0.015 K and the I-V curves are measured.

Standard cryogenic filtering techniques lower the electron temperature. Differential conductance is obtained using a lock-in technique. The applied voltage is a sum of a constant dc-voltage V and a weak ac-voltage $v(t) = v_{AC}\sin(2\pi ft)$, where $v_{AC} = 1\mu$ V and $f = 500$ Hz. Current I is measured with an Ithaco current preamplifier. To obtain the differential conductance, the output of the amplifier is connected to the input of a lock-in amplifier.

The effects of the gate voltage on differential conductance are shown in fig 5, at $T = 0.015K$ in sample 3. The differential conductance near zero bias voltage is strongly suppressed. If the bias voltage aproaches a certain threshold from below, the differential conductance rapidly increases by several orders of magnitude.

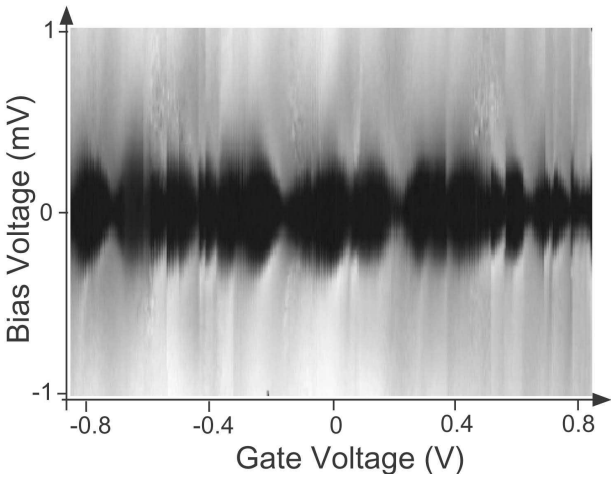

FIG. 5: Gate voltage dependence of the Coulomb blockade, in sample 3. Darker = smaller conductance. The diamonds represent different charged states of the grain, analogous to the gate voltage dependences in quantum dots. [13]

The voltage threshold displays quasiperiodic modulation with the gate voltage. By applying the gate voltage, the voltage threshold can be reduced to zero. If the gate voltage is chosen so that the voltage threshold is at maximum, then the conductance at zero bias voltage is four orders of magnitude smaller than the conductance at large bias voltage.

This proves unambiguously that the sample consists of a metallic grain connected to drain and source, rather than a single junction. The diamonds in Fig. 5 are symmetric around zero bias voltage, showing that $C_L \approx C_R$, where $C_{L,R}$ are the effective capacitances determined from the fit to the Orthodox theory of single-charge tunneling on a single metallic island. [22] The image is chopped, because of the random switches in the background charge distribution (note that the gate voltage range is rather large compared with the bias voltage).

Figure 6-A shows the I-V curve of sample 1. This I-V curve is typical for our high resistance samples. We fit the I-V curve using the Orthodox theory, [22] and show the corresponding fit by the dashed line. Good fits are generally found in approximately 50% of the samples, suggesting that the samples typically consist of a single metallic grain in weak electric contact with the drain and the source.

The charging energy 82 meV extracted from the fitting is relatively large. As a result, the bias voltage can induce jumps in the background charge distribution (also known as Q_0-shifts in the Orthodox theory). The I-V curve of sample 1 displays a noticeable deviation from the fit

TABLE I: $R_L + R_R$, R_L/R_R , $C_L + C_R$, C_L/C_R: junction resistances and capacitances determined from the Coulomb staircase, in samples 1,2, and 3, and from the theory of strong tunneling in an SET, in sample 4. In samples 1-3, the capacitances are effective, and in sample 4, the capacitance is bare. E_C is the effective charging energy.

	$R_L + R_S[k\Omega]$	R_L/R_S	$C_L + C_S[aF]$	C_L/C_S	$E_C[meV]$
1	550	2.9	0.98	1.2	82
2	344	1	17.4	1	4.6
3	56	1	410	1	0.2
4	14	7.1	5.52	-	$\ll 0.1$

at positive bias voltage, see Fig. 6-A. These deviations are not noise. They are hysteretic - they change when sweeping the voltage up and down. At negative voltage bias, the deviations from the fit are weak and we do not observe any hysteresis when repeating the voltage sweep. This behavior is thus far consistent with single charge tunneling.

Among samples, charging energy fluctuates strongly. These fluctuations are explained by the broad distribution of particle diameters possible in such systems, Fig. 4. In addition, there is another source of fluctuations in charging energy, caused by the distribution of contact conductances. This effect will be discussed in the next section.

INTERMEDIATE COULOMB BLOCKADE

As $R_L + R_R$ decreases, the effective charging energy rapidly approaches zero, as shown in table 1. If the gap in the $I-V$ curve is well resolved at $T = 0.015K$, the grains are referred to as closed. The range of conductances of closed grains is indicated in Fig. 2-B. In table 1, samples 1-3 display a clear Coulomb blockade at $T = 0.015K$. The parameters in these samples are obtained from the fits to the orthodox theory.

Figure 6-B shows $I-V$ and $dI/dV-V$ curves in sample 2. This sample displays a sharp Coulomb blockade, similar to that in sample 1. The I-V curve has no hysteresis, which is not surprising, since the charging energy is only 4.6 meV and the bias voltage is too weak to reconfigure the background charge distribution. The Orthodox theory is in good agreement with the linear segments of the I-V curve. We can identify the same threshold voltages at both signs of the bias voltage: (a) corresponds to (d) and (b) corresponds to (c). This confirms there is only one grain in series with drain and source.

The rounding of the I-V curve is larger than expected from the Orthodox theory. A good fit is obtained with identical junction parameters $R_L = R_R$ and $C_L = C_R$. The first identity, $R_L = R_R$, is not as important as the second identity; good fits can be obtained even if

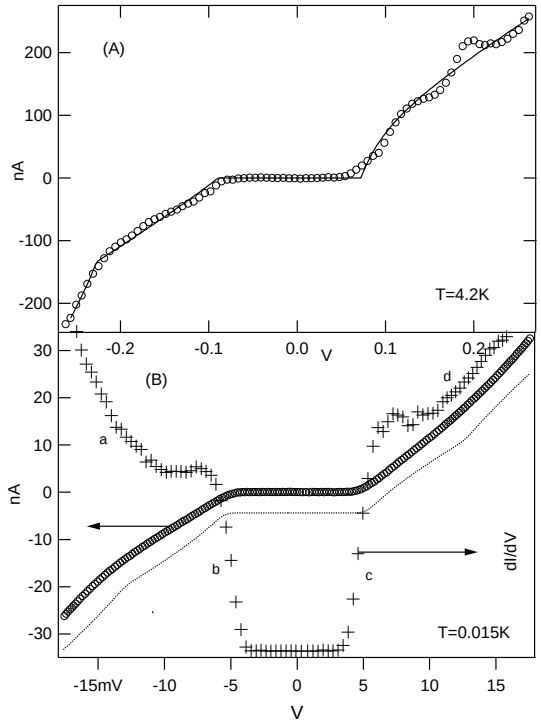

FIG. 6: A. Circles: I-V curve of sample 1. Line: fit to the Coulomb staircase on single grain obtained from the Orthodox theory. The charging energy $E_C = 82meV$. B. Circles: I-V curve of sample 2. Crosses: differential conductance versus voltage. Line: fit to the Orthodox theory. The line is offset in vertical direction for clarity. The best fit parameters determine effective capacitances, not the geometric capacitances, as described in the text.

$R_L/R_R \neq 1$. $C_L = C_R$ follows directly from the I-V curve, from the fact that the threshold voltages (b) and (c) have the same magnitude. We have noticed this symmetry in contact capacitance in a relatively large number of samples - roughly 50% of samples with charging energy less than 5 meV. In samples with $E_C < 1$ meV, this symmetry is found in nearly every sample studied.

We do not have an explanation for this symmetry at low temperature and low bias voltage. Experimentally, no special care has been taken to make the junctions symmetric. In fact, the parameters are expected to be significantly asymmetric. We note that the symmetry in effective capacitance is broken in a strong magnetic field. The discussion of the magnetic field dependence is beyond the scope of this paper.

Theoretically, one expects that if $G_L + G_R > G_0$, where $G_{L,R} = 1/R_{L,R}$, the system parameters become renormalized near zero temperature and zero bias voltage. The effective charging energy of the grain decays exponentially with contact conductance,

$$E_C^{eff} = E_C e^{-\alpha(G_L+G_R)/G_0}, \qquad (1)$$

where α is a constant of order 1, dependent on the na-

ture of the contacts ($\alpha = 1$ in tunneling junction and $\alpha = \pi^2/4$ in a diffusive metallic contact), E_C is the bare charging energy. [23, 24] This exponential dependence on G_L and G_R also explains strong fluctuations in the charging energy among samples.

The suppression of Coulomb blockade have been studied in larger metallic SETs. [25, 26] The connection between the effective charging energy and the bare sample parameters have been established. [25] Our samples are different from metallic SETs in that the contacts are metallic, and the grain diameter is small - small enough so that an electron can enter and exit the grain without loosing its phase coherence. [33]

No calculation of the $I-V$ curve in this regime is available. We still fit the $I-V$ curve using the Orthodox theory, with the notion that the best fit parameters represent effective (renormalized) parameters. In this sense, $E_C^{eff} = e^2/(2C^{eff})$. The central result of this paper, beyond describing the new technique, is that $C_L^{eff} = C_R^{eff}$, when $E_C^{eff} \ll E_C$ and when the applied magnetic field is weak. In table 1, the sample parameters are the effective parameters as defined here. No connection between effective and bare parameters is established in this paper. This connection is the subject of present research in our laboratory.

The observation $C_L^{eff} = C_R^{eff}$ has important implications for conversion from bias voltage into grain energy. For example, if the density of states of the grain varies as a function of energy, then this variation can be measured from the I-V curve. The capacitive division prefactor, which converts from bias voltage to energy, is 2.

In instances where the theoretical calculations can be solved exactly, the theory predicts that any asymmetry in the junction's real parameters is only enhanced by the renormalization at low temperatures and low bias voltage. [27] The theoretical model, however, is valid only if there is one electronic mode per contact, which may not apply to our samples. Our data demonstrate the *opposite* behavior from that predicted theoretically: in a weak magnetic field, the effective capacitances are symmetrized.

WEAK COULOMB BLOCKADE

We have observed that when the sample resistance at room temperature is less than roughly $10k\Omega$, then the conductance at $T = 0.015K$ near zero bias voltage remains on the same order of magnitude as the conductance at large bias voltage (asymptotic conductance/resistance). In Fig. 2-B, the grains with this property are referred to as open. Fig. 7 shows dI/dV versus V in a sample with room temperature resistance $\approx 14k\Omega$. We observe that the conductance at $V = 0$ and $T = 0.015K$ remains within an order of magnitude

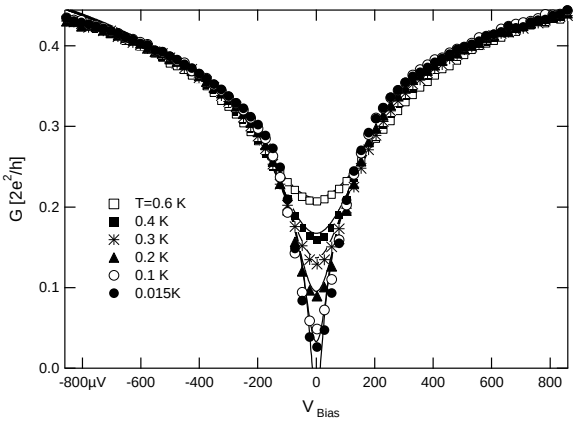

FIG. 7: Symbols: Differential conductance versus bias voltage in sample 3 as a function of temperature. Lines: Fit to the theory of strong tunneling in a metallic grain.

from the room temperature conductance. In samples with asymptotic resistance $10k\Omega < R_L + R_R < 20k\Omega$, the depth and the width of the conductance dip fluctuates strongly among samples (in two out of forty samples studied thus far, the conductance dip is significantly less pronounced than that in Fig. 7).

As the temperature increases, the zero-bias dip broadens. While at room temperature, the zero bias conductance dip is no longer resolved; the I-V becomes linear, with the conductance equal to the $1/(R_L + R_R)$. Alternatively, this asymptotic conductance is obtained at low temperatures, by applying a large enough bias voltage so that the I-V curve approaches the linear form.

To interpret this result we first try to fit the data in Fig. 7 to the dynamic Coulomb blockade model of a single tunneling junction. [28, 29] Yeyati et al. have extended this model to include a metallic contact with one channel, [30] showing that the temperature dependence of a metallic contact does not differ from that of a tunneling junction. Fitting to the dynamic Coulomb blockade model does not reproduce the temperature dependence in Fig. 7.

We fit the data in Fig. 7 to the theory of a mesoscopic metallic grain in the strong tunneling limit. [31] This theory has already been used in connection with measurements of strong tunneling SETs by Chouvaev et al. [26] Strictly speaking, the model in Ref. [31] is not applicable to our devices because our contacts are metallic. For example, the parameter α in Eq. 1 differs between metallic contacts and tunneling contacts by a factor of $\pi^2/4 = 2.46$. This implies that the Coulomb blockade is much more strongly suppressed with metallic contacts than with tunneling contacts. [24]. In the absence of a theory of the I-V curve for a grain with metallic contacts, we use the theory of tunneling contacts. [31] The theory is valid only if $eV \gg E_C^{eff}$ or $k_BT \gg E_C^{eff}$.

The I-V curve is

$$I(V) = \frac{V}{R_L+R_R} - \frac{e}{\pi\hbar}\frac{R_L R_R}{(R_L+R_R)^2}\,\mathrm{Im}\sum_{r=L,R} \left(\frac{\hbar}{R_0 C} + ieV_r\right)\Psi\left(1+\frac{\hbar}{2\pi k_B T R_0 C} + i\frac{eV_r}{2\pi k_B T}\right) - ieV_r\Psi\left(1+i\frac{eV_r}{2\pi k_B T}\right) \quad (2)$$

Here $R_0 = \frac{R_L R_R}{R_L+R_R}$, $C = C_L + C_R$, $V_L = \frac{R_L}{R_L+R_R}V$, $V_R = \frac{R_R}{R_L+R_R}V$ and $\Psi(x)$ is the digamma function. Note that there is a misprint in Ref. [31]. The corrected expression is given in Ref. [26].

There are three fitting parameters R_L, R_R and C. We set $R_L + R_R$ to be the same as the sample resistance at high temperature/voltage, and vary C and R_L/R_S to obtain the best fit. We fit the family of dI/dV vs V curves measured at different temperatures. The best fit is shown by lines in Fig. 7, and the corresponding sample parameters are given in Table 1, for sample 3. The fit reproduces our data quite well in the entire temperature range.

The I-V in Eq. 2 does not depend on on the capacitance ratio C_L/C_R. It is reasonable to assume that if the conductance at $V = 0$ and $T = 0.015K$ is several times smaller than $1/(R_L + R_R)$, then the voltage division across the grain is closer to capacitive than resistive. Then, if Eq. 2 holds, it follows that the effective capacitive division is independent on the bare capacitance ratio C_L/C_R. This may partially explain why the measured capacitances in the intermediate Coulomb blockade regime are identical.

CONCLUSION

In conclusion, we present a new technique for fabrication of metallic grains in contact with leads. These grains are connected by two metallic atomic-scale point contacts, with well transmitted conduction channels. We show that when the sample resistance at room temperature is above h/e^2, then the $I-V$ curve at low temperatures displays the Coulomb blockade. When the sample resistance approaches h/e^2, the blockade is weakened. We discover an intermediate regime in which the I-V curve is described by the Coulomb staircase with symmetric junction capacitances. As the sample resistance is reduced further, the Coulomb blockade is completely washed out, and only a weak zero bias conductance dip is observed. This regime is well described by the theory of metallic grains with strong tunneling.

We thank M. Pustilnik, L. P. Kouwenhoven, D. Golubev for useful discussions. We thank the Georgia-Tech electron microscopy facility where electron transport experiments in combination with sample imaging have been performed. This work was performed in part at the Cornell Nanofabrication Facility, (a member of the National Nanofabrication Users Network), which is supported by the NSF, under grant ECS-9731293, Cornell University and Industrial affiliates. This research is supported by the David and Lucile Packard Foundation grant 2000-13874 and the NSF grant DMR-0102960.

* dragomir.davidovic@physics.gatech.edu

[1] U. During, O. Zuger, , and D. W. Pohl, Phys. Rev. Lett. **65**, 349 (1990).
[2] J. Moreland and J. W. Ekin, J. Appl. Phys. **58**, 3888 (1985).
[3] C. J. Muller, J. M. van Ruitenbeek, and L. J. de Jongh, Physica C **191**, 485 (1992).
[4] B. J. van Wees, H. van Houten, C. W. J. Beenakker, J. G. Williamson, L. P. Kouwenhoven, D. van der Marel, and C. T. Foxon, Phys. Rev. Lett. **60**, 848 (1988).
[5] D. A. Wharam, T. J. Thornton, R. Newbury, M. Pepper, H. Ahmed, J. E. F. Frost, D. G. Hasko, D. C. Peacock, D. A. Ritchie, and G. A. C. Jones, J. Phys. C **21**, L209 (1988).
[6] U. Landman, W. D. Luedtke, N. A. Burnham, and R. J. Colton, Science **248**, 454 (1990).
[7] A. P. Sutton and J. B. Pethica, J. Phys.: Condens. Matter **2**, 5317 (1990).
[8] D. C. Ralph, C. T. Black, and M. Tinkham, Phys. Rev. Lett. **74**, 3241 (1995).
[9] D. Davidović and M. Tinkham, Phys. Rev. Lett. **83**, 1644 (1999).
[10] T. A. Fulton and G. J. Dolan, Phys. Rev. Lett. **59**, 109 (1987).
[11] M. A. Kastner, Rev. Mod. Phys. **64**, 849 (1992).
[12] R. C. Ashoori, Nature **379**, 413 (1996).
[13] L. P. Kouwenhoven, C. Marcus, P. McEuen, S. Tarucha, R. Westervelt, and N. Wingreen, in *Mesoscopic Electron Transport*, edited by L. P. Kouwenhoven, L. L. Sohn, and G. Schon (Elsevier and Amsterdam, 1997), p. 549.
[14] N. Agrait, A. L. Yeyati, and J. V. Ruitenbeek (????), cond-mat/0208239.
[15] J. V. Delft and D. C. Ralph, Phys. Rep. **345**, 61 (2001).
[16] H. Park, A. K. L. Lim, A. P. Alivisatos, J. Park, and P. L. McEuen, Appl. Phys. Lett. **75**, 301 (1999).
[17] J. Park, A. N. Pasupathy, J. I. Goldsmith, C. Chang, Y. Yaish, J. R. Petta, M. Rinkoski, J. P. Sethna, H. D. Abruna, P. L. McEuen, et al., Nature **417**, 722 (2002).
[18] T.M.Mayer, J.E.Hueston, G.E.Franklin, A.A.Erchak, and Michalske, Jour. Appl. Phys. **85**, 8170 (1999).
[19] K. Hansen, S. K. Nielsen, M. Brandbyge, E. Laegsgaard, I. Stensgaard, and F. Besenbacher, Appl. Phys. Lett. **77**, 708 (2000).
[20] K. Hansen, S. K. Nielsen, E. Laegsgaard, I. Stensgaard, and F. Besenbacher, Rev. Sci. Instrum. **71**, 1793 (2000).
[21] E. L. Wolf, *Principles of Electron Tunneling Spectroscopy* (Oxford University Press, 1989).
[22] D. V. Averin and K. K. Likharev, in *Mesoscopic Phenomena in Solids*, edited by B. L. Altshuler, P. A. Lee, and R. A. Webb (Elsevier, NY, 1991), p. 173.
[23] S. V. Panyukov and A. D. Zaikin, Phys. Rev. Lett. **67**,

3168 (1991).
[24] Y. V. Nazarov, Phys. Rev. Lett. **82**, 1245 (1999).
[25] P. Joyez, V. Bouchiat, D. Esteve, C. Urbina, and M. H. Devoret, Phys. Rev. Lett. **79**, 1349 (1997).
[26] D. Chouvaev, L. S. Kuzmin, D. S. Golubev, and A. D. Zaikin, Phys. Rev. B **59**, 10599 (1999).
[27] A. Furusaki and K. A. Matveev, Phys. Rev. Lett **75**, 709 (1995).
[28] M. H. Devoret, D. Esteve, H. Grabert, G. L. Ingold, H. Pothier, and C. Urbina, Phys. Rev. Lett **64**, 1824 (1990).
[29] S. M. Girvin, L. I. Glazman, M. Johnson, D. R. Penn, and D. Stiles, Phys. Rev. Lett **64**, 3183 (1990).
[30] A. L. Yeyati, A. Martin-Rodero, D. Esteve, and C. Urbina, Phys. Rev. Lett. **87**, 046802 (2001).
[31] D. S. Golubev, J. Konig, H. Schoeller, G. Schon, and A. D. Zaikin, Phys. Rev. B **56**, 15782 (1997).
[32] In a separate publication, we examine the effect of water molecules on the I-V curve in Fig. 2-A in detail. We find that water is an excellent insulator: when water vapor pressure is increased, the barrier height increases, increasing the sample resistance by orders of magnitude.
[33] The traversal time is roughly $((R_L+R_R)/R_Q)h/\delta$, where δ is the level spacing and $R_Q = h/e^2$. For a grain of diameter 20nm, the traversal time is easily shorter than the dephasing time in pure gold at low temperatures.